To be published in Optics Letters:

Title: Holographic Fourier Transform Spectrometer for THz Region
Authors: Nikolay Agladze and Albert Sievers
Accepted: 6 January 2010
Posted: 26 January 2010
Doc. ID: 118783

Holographic Fourier Transform Spectrometer for THz Region

N. I. Agladze and A. J. Sievers

Laboratory of Atomic and Solid State Physics

Cornell University

Ithaca, NY 14853-2501, USA

Because of the development of detector arrays stationary interferometric spectrometers now have many applications in the visible and IR; however, these same array sizes make it impractical to design a single Fourier optics system with the necessary large field angles required for the THz region. By dividing the Fourier optics into independent components in each arm of an interferometer we show that the aberrations are dramatically reduced, while maintaining the same theoretical throughput as the scanning Michelson interferometer.

OCIS codes*: 220.1000; 220.4830; 260.3160; 300.6300*

One of the most pressing issues in accelerator science today is the production of sub-picosecond duration electron bunches. Such bunches are required for a broad spectrum of applications, from achieving high luminosity in a linear collider to generating short duration X-ray pulses [1, 2]. Means to measure the temporal distribution of charge within a single bunch on a bunch-by-bunch basis are required to make progress in this direction. One approach was demonstrated recently based on transverse deflecting microwave structures [3]. Another economical non-destructive method is based on detection of the coherent synchrotron or transition radiation produced by the short electron bunch since it contains detailed information about the bunch shape [4]. To measure the coherent spectrum from single bunches we have designed and built a miniature holographic Fourier transform spectrometer coupled with a commercial far IR detector array. Real time bunch shape diagnostics becomes possible with this new technique.

In a holographic Fourier transform spectrometer (HFTS) the static interferogram is created in the spatial domain and is sampled with the multichannel detector. Because of the development of detector arrays HFTS now have many applications in the visible and IR when compact size, broad bandwidth, large optical throughput, and characterization of time dependent sources are required. A shearing interferometer is often employed in the visible since its fringe visibility does not depend on the size of the source [5] thereby ensuring a high throughput. In the visible version of the instrument the source and the array detector are located at the same focal length from the lens providing a Fourier lens (or Fourier concave mirror for reflecting optics). However for a realistic detector array size it is not possible to design an aberration corrected Fourier optical system with the necessary large field angles required for the THz region.

By dividing the Fourier system into independent components in each arm of an interferometer we dramatically reduce the aberrations enabling a high throughput THz HFTS. This solution is superior to dividing the beams after the single Fourier component and recombining them on the array with a set of flat mirrors as, say, in a modified Mach-Zehnder interferometer [6]. Our design described here preserves a high throughput since it minimizes the focal distance of the Fourier optics. With the finite source the effective overlap of the collimated beams on the array requires that the source and the array are located at focal distances from the Fourier lens which is impossible to realize with such interferometers as the Mach-Zehnder unless the focal length is very large. Our design will operate both with coherent and incoherent sources unlike some autocorrelators that make use of the transverse coherence of the transition radiation [7, 8].

Division of the Fourier system into separate parts is possible both for shearing and tilt interferometers; but for the large interference angle required the tilt interferometer has more symmetric optics compared to the shearing interferometer so the aberrations are easier to control. In Fig. 1 is shown the equivalent geometry of the holographic FTS for the THz region. Two virtual sources created by the tilt interferometer, A_1 and A_2 correspond to the same off-axis point and are characterized by an identical set of field coordinates (x_i, y_i), $i = 1,2$. These two virtual sources are located at the focal planes of Fourier lenses L_1 and L_2, with interference angle α. Collimated beams with wave vectors $\mathbf{k}_1$ and $\mathbf{k}_2$ created by the lenses overlap at the 2D array detector plane (xy in Fig. 1). Field angles ψ and φ correspond to out of plane and in plane positions and also describe directions of the corresponding wave vectors $\mathbf{k}_1$ and $\mathbf{k}_2$. The calculation of the intensity distribution for a fixed field position in the detector (x,y) plane is done for the transverse incoherent case. Wave vectors $\mathbf{k}_1$ and $\mathbf{k}_2$ both make angle ψ with the yz

plane and their directions in this plane are described by angles $\alpha/2+\varphi$ and $-\alpha/2+\varphi$, respectively. First the calculations are performed for monochromatic light and then the total intensity is obtained by integrating over the spectral density $B(\sigma)$. Assuming the amplitude transmission and reflection coefficients τ and $1-\tau$ at the beamsplitter for a specific polarization analyzed by the detector, the intensity produced in the detector plane (xy) is given by the following relation

$$I(x,y)=\int_0^\infty I^0(\sigma,x,y)\left\{\tau^2+(1-\tau)^2+2\tau(1-\tau)\cos\left[(2\pi\sigma y)2\sin(\alpha/2)\cos\varphi\cos\psi\right]\right\}B(\sigma)d\sigma, \quad (1)$$

where $I^0(\sigma,x,y)$ is the intensity at frequency $\sigma\equiv 1/\lambda$ (λ is the wavelength) in the absence of the beamsplitter. The product of cosine factors is equal to the single cosine of angle Θ between the wave vector and the axial direction, identified in Fig. 1. The effect of the cosine factor results in a frequency shift in the opposite direction when compared to that found for the scanning FTS but in the second order approximation the same relation $\Omega R\le 2\pi$ (Ref. [9], page 149] is valid for the resolving power $R=\sigma_{\max}/\delta\sigma$ (ratio of the maximum non-aliased frequency $\sigma_{\max}$ to the spectral resolution $\delta\sigma$) of the spectrometer and the solid angle Ω subtended by the circular source observed from the center of the Fourier component (shown in Fig. 1 as a cone with the vertex at L_1). Notable is the absence of the x coordinate dependence – for the ideal Fourier system in each arm of the tilt interferometer there is no distortion of the fringes. In many cases the frequency dependence of the factor $I^0(\sigma,x,y)$ can be neglected (or factored out and included in $B(\sigma)$) resulting in a relation similar to the one for the scanning interferometer. The scaling factor for the static interferogram produced at the array detector is $2\sin\alpha/2$. It corresponds to the

scaling factor δ/f for the visible shearing HFTS[5] and all operating parameters of the instrument can be calculated in the same way with the new scaling relation.

Key elements of the THz HFTS are the Fourier optical components in its two arms. In the present instrument two commercially available 30° off-axis parabolic mirrors are chosen with the parent focal length 254 mm and the diameter 50 mm. The size of the array detector (Pyrocam III made by Spiricon) with 124 x 124 elements is 12.4 mm and is sufficiently small for the diffraction at the mirror edge not to affect the interference pattern for wavelengths 3 mm and shorter. In Fig. 2 is shown the top view of the optical layout of the THz HFTS. The main purpose of the interferometer is to produce two virtual sources tilted by an angle of $\alpha = 25°$ with respect to the axial point at the detector. A 45° off-axis parabolic mirror (1) accepts the collimated beam and focuses it slightly behind the wire grid beamsplitter (2). In this way the beamsplitter size is setting the acceptance angle of the instrument. Both reflected and transmitted beams are directed to corresponding tilted mirrors (5) and (6), which send the radiation to the 30° off-axis parabolic reflectors (7) and (8) (corresponding to lenses L_1 and L_2 in Fig. 1). After collimation by the reflectors the beams are combined at the array detector. The polarizer (9) at 45° is used to mix the orthogonal polarizations propagating along the two arms of the interferometer. Shutters (3) and (4) are used to measure independently the intensity distributions at the array produced by each of the interferometer arms. The array detector characteristics set the maximum frequency $\sigma_{\max} = 118\,cm^{-1}$ and the resolution $\delta\sigma > 1.1 cm^{-1}$.

A sufficiently large field of view of the spectrometer is one of the main requirements in the design process. Ray tracing is used to verify the aberration compensation of the instrument. The interference pattern at the detector was calculated using the ray tracing software ZEMAX in a non-sequential mode by tracing 10 million rays at frequency 30 cm^{-1} for each angle. Maximum

values for angles $-40\ mrad \le \varphi \le 40\ mrad$ and $-45\ mrad \le \psi \le 45\ mrad$ are given by vignetting on the beamsplitter. In order to characterize aberration characteristics of the interferometer more quantitatively the interference patterns for all oblique directions were converted into interferograms by summing up all pixels along *x* directions. Frequencies of the spectra calculated from the interferograms are shown in Fig. 3 as functions of the oblique angles φ and ψ. As expected from Eq. 1 the frequency shift is the same for both field directions. The solid line in the figure shows the frequency change with the field angle for ideal Fourier components. The ray tracing result is that aberrations of the real interferometer do not exceed the ideal field dependence. The dashed line represents the field dependent frequency shift for the scanning FTS, which is equal in absolute value, but has opposite sign.

Vignetting is the main factor limiting the throughput of the instrument in the low frequency region. The following analysis compares the interferometer with the ideal HFTS depending on the number of elements in the array. The resolving power of the THz HFTS for the array with $N = 124$ elements is [5] $R < N/1.204 \approx 100$. The acceptance angle $\Omega = 0.0059\,srad$ as determined by the vignetting. The product $R\Omega < 0.59$, which is about an order of magnitude less than the ideal value 2π. By using a detector of the same size but with ten times more elements (1240) the throughput of the existing instrument would match the ideal value. In this case the maximum non-aliased frequency would not be $\sigma_{\max} = 118\,cm^{-1}$ as for the Pyrocam detector but $10 \times \sigma_{\max} = 1180\,cm^{-1}$. This cutoff frequency is quite feasible with existing thin film polarizing beamsplitters. Only arrays with the uniform broadband efficiency, number of elements ~ 1000, and pitch size ~ 12 μm are needed to cover this region with a resolution of $\sim 1.2\,cm^{-1}$.

In conclusion the important elements of this design are: (1) using a split Fourier system in the tilt interferometer to radically reduce field aberrations; (2) showing that the theoretical

throughputs of the current HFTS and of the Michelson scanning FTS are equal; and (3) demonstrating that vignetting is the main throughput limiting factor for the designed THz HFTS.

Acknowledgments

Work supported by DOE-DE-FG02-04ER46154. The use of facilities of the Cornell Center for Material Research (supported by NSF Grant DMR 0520404) is also acknowledged.

References

1. S. M. Gruner, D. Bilderback, I. Bazarov, K. Finkelstein, G. Krafft, L. Merminga, H. Padamsee, Q. Shen, C. Sinclair, and M. Tigner, "Energy recovery linacs as synchrotron radiation sources (invited)," Review of Scientific Instruments **73**, 1402-1406 (2002).
2. D. H. Bilderback, P. Elleaume, and E. Weckert, "Review of third and next generation synchrotron light sources," Journal of Physics B-Atomic Molecular and Optical Physics **38**, S773-S797 (2005).
3. M. Röhrs, C. Gerth, H. Schlarb, B. Schmidt, and P. Schmüser, "Time-resolved electron beam phase space tomography at a soft x-ray free-electron laser," Physical Review Special Topics-Accelerators and Beams **12**, 0507041-05070413 (2009).
4. D. Mihalcea, C. L. Bohn, U. Happek, and P. Piot, "Longitudinal electron bunch diagnostics using coherent transition radiation," Phys. Rev. ST Accel. Beams **9**, 0828011-0828017 (2006).
5. N. I. Agladze and A. J. Sievers, "Miniaturization of holographic Fourier-transform spectrometers," Applied Optics **43**, 6568-6579 (2004).
6. M. L. Junttila, J. Kauppinen, and E. Ikonen, "Performance Limits of Stationary Fourier Spectrometers," Journal of the Optical Society of America a-Optics Image Science and Vision **8**, 1457-1462 (1991).
7. D. Sütterlin, V. Schlott, H. Sigg, D. Emi, H. Jäckel, and A. Murk, "Spatial auto-correlation interferometer with single shot capability using coherent transition radiation," in *DIPAC 2005,* (CERN, Lyon, France, 2005), pp. 211-213.

8. G. Andonian, S. Boucher, P. Frigola, A. Murokh, and G. Travish, "A real-time bunch length terahertz interferometer," in *EPAC 2008,* I. Andrian, O. Brüning, Petit-Jean-Genaz, and P. Pierini, eds. (EPS-AG, Genoa, Italy, 2008), pp. 1218-1220.

9. R. J. Bell, *Introductory Fourier transform spectroscopy* (Academic Press, New York, 1972).

Figure Captions

Figure 1. Simplified geometry for a tilt interferometer based holographic FTS. Two arms of the interferometer contain separate Fourier lenses L_1 and L_2 which are located at focal length f both from the corresponding virtual sources created by the interferometer (x_i, y_i), $i = 1, 2$ and from the array detector (x, y). The off-axis point at the source is represented by the pair of points A_1 and A_2 and is described by field angles ψ and φ for out of plane and in plane directions correspondingly. Wave vectors $\mathbf{k}_1$ and $\mathbf{k}_2$ correspond to collimated beams interfering at the angle α in the detector plane.

Figure 2. Top view of the THz tilt interferometer. 1 – fore optics (45° off-axis parabolic mirror); 2 – beamsplitter; 3,4 – shutters; 5,6 – out-of-plane tilted mirrors; 7,8 – two halves of the split Fourier system (30° off-axis parabolic mirrors, under the platform); 9 – polarizer in front of the detector.

Figure 3. Frequency shift for oblique directions. Dashed line is for scanning FTS and solid line is for holographic FTS with ideal Fourier optics. The shifts have opposite signs but the same absolute values for these instruments. Open circles and squares are for the designed THz interferometer with 30° off-axis parabolic reflectors and split Fourier system for in the plane (φ) and out of the plane (ψ) field directions correspondingly. Ray tracing confirms that the actual field aberrations do not exceed ideal values for holographic FTS.

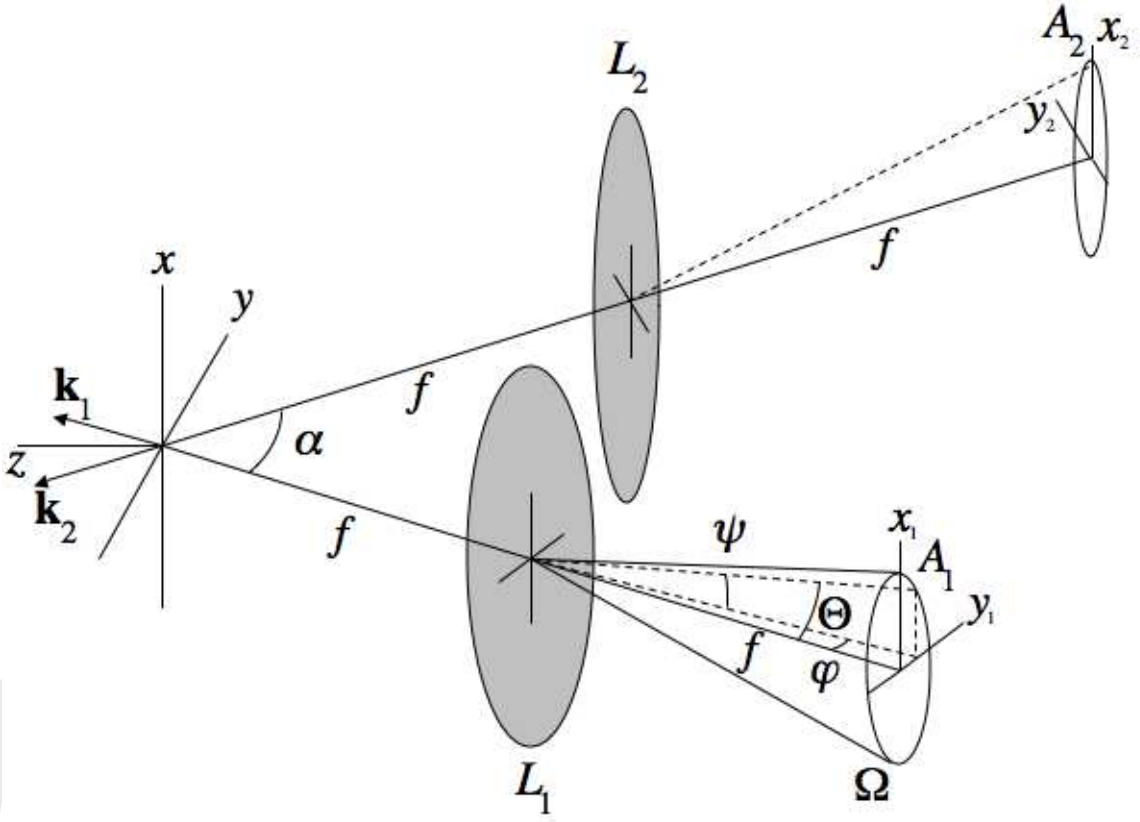

Figure 1.

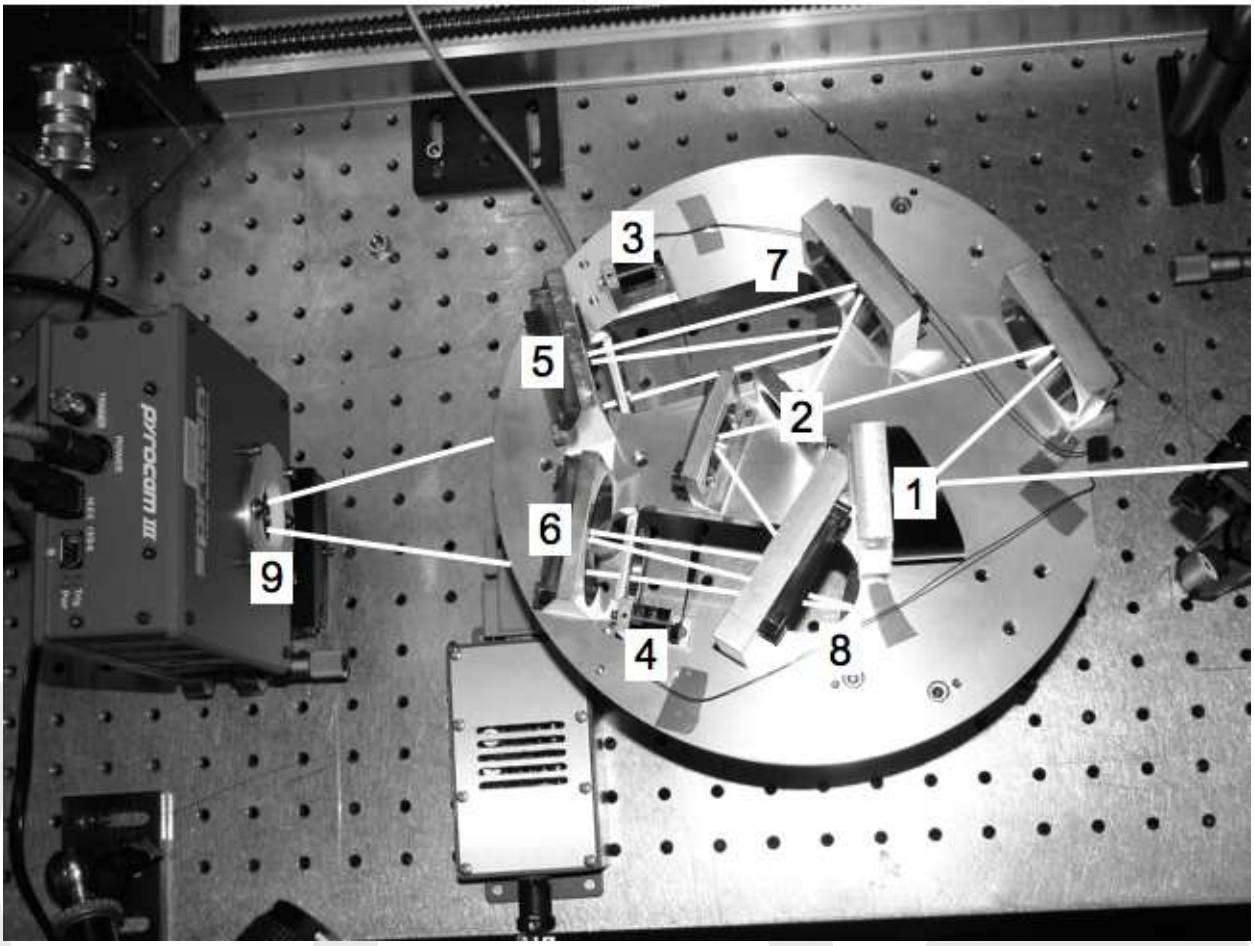

Figure 2.

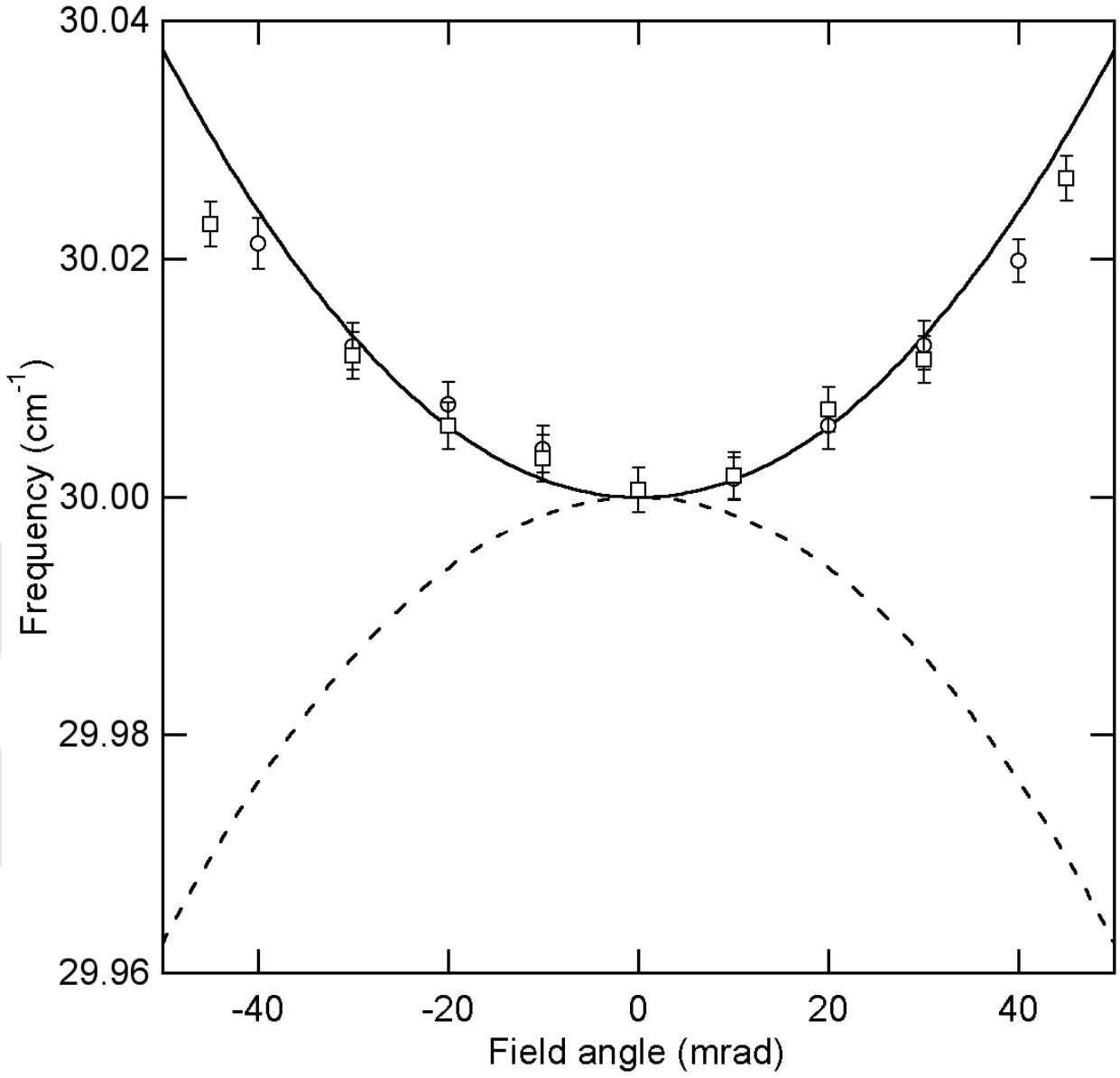
30.04
30.02
30.00
29.98
29.96
Frequency (cm-1)
-40
-20
0
20
40
Field angle (mrad)

Figure 3.